DOI: 10.13009/EUCASS2019-613

Prediction of Subscale Rocket Engine Acoustic Emissions Using CAA Hybrid Methods

E. Costa Ruiz†, R. Stark, S. General and M. Oschwald
German Aerospace Center (DLR)
Langer Grund, 74239 Hardthausen, Germany
eugeni.costaruiz@dlr.de
†Corresponding author

Abstract

This work presents the results of a numerical study predicting the acoustical emissions induced by the supersonic jets of two different types of nozzle using a CAA (Computational Aeroacoustics) hybrid method. The two types of nozzles studied are a Truncated Ideal Contour (TIC) and a Thrust Optimized Parabola (TOP). To achieve this goal two test series were conducted with the TIC and the TOP nozzle. The results show that the quality of the results depend on the direction in which it is measured. The agreement between experiments and simulation are good in the areas where the underlying model expects it.

1. Introduction

Acoustic emissions are a key issue during rocket engine starts. The payload of the rocket and the rocket self are sensitive to high acoustic loads. Therefore it is very valuable to be able to predict acoustic emissions before a rocket engine starts for the first time. The acoustic loads on payload and rocket depend on some factors like intensity of the acoustic source, the geometry surrounding the source, or the weather. Rocket engine test benches are more robust and less sensitive to high acoustic loads, however if the test bench is near a populated area, legal acoustic emission restrictions have to be taken into account. In this case the prediction of the acoustic emission before the tests are performed is a very appreciated information, specially during the licensing process of a new test bench. It is possible to predict acoustic loads using high fidelity methods like Direct Numerical Simulation (DNS) or Large Eddy Simulation (LES) but these have prohibitive costs. A more cost efficient way is to use Computational Aeroacustics (CAA) hybrid methods. An example of CAA hybrid methods for lift-off acoustic was applied by Tsutsumi and Terashima[11] by combining LES/RANS (Reynolds Averaged Navier Stokes) for characterizing the free jet in a first step and then later using the full Euler Equations in a CAA computation to obtain the acoustic load distribution in the launch pad. The method[4] used in this work was developed for the use cases of the aeronautic sector and bases on the model of Tam and Auriault.[1] It is validated for Mach numbers up to 2. This method uses a two step approach using a RANS simulation for characterizing acoustic sources and then a CAA computation using Linearized Euler Equations (LEE) to calculate the acoustic distribution. A first application for a cold gas sub scale rocket engine with exit Mach number of 5 was presented by Costa et al.[3] However in the experiment only three microphone positions were measured. According to Tam and Auriault[1] the model produces good results in the area 50° to 110° from the nozzle exit (see Figure 1). The main goal of this work is to check if the model of Tam and Auriault[1] produces good results as well, for Mach numbers higher than 2. The experiments simulated in this work were measured with 11 microphones, so a much better evaluation between simulation and experiment regarding the directivity can be realized. Two cold gas test cases were simulated, a Truncated Ideal Contour (TIC) and a Thrust Optimized Parabola (TOP). Although both cases have different nozzle profiles they have similar operation parameters. For the detailed experimental study refer to the to Stark et al.[9]

2. Methodology

The method used in this work is a two-step approach. In a first step a normal RANS simulation is performed. From this simulation turbulence statistics are gathered in order to generate the acoustic sources. The RANS simulations were performed with the DLR Solver Tau.[7]

DOI: 10.13009/EUCASS2019-613

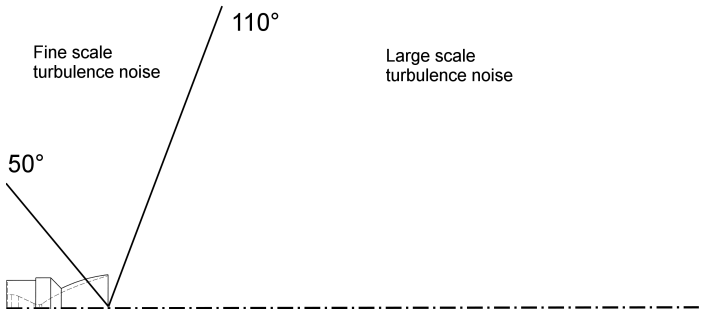

Figure 1: Area between 50° and 110° is the area where the T&A model produces best results

2.1 Acoustic Modelization

The acoustic sources are defined as a source term in the LEE. The source term is defined in the right hand side of the LEE pressure equation, the continuity equation of the LEE is not considered because the mean flow gradients are neglected,

$$\begin{aligned} &\rho_0\Big[\tfrac{\partial u'}{\partial t} + u_0\nabla u'\Big] + \nabla p = 0 \\ &\tfrac{\partial p}{\partial t} + u_0\nabla p + \gamma p_0 \nabla u' = q_p. \end{aligned} \tag{1}$$

The acoustic sources are obtained using the Random Particle-Mesh (RPM) method.[4] This method has been used for simulating acoustics of subsonic stream jets, for a more detailed description of the method refer to the work of Neidfeld and Ewert.[8] The RPM method uses the turbulence statistics to model the intensity of spatially and temporally fluctuating quantities which are moving with the underlying jet mean jet velocity. The noise prediction model of the RPM method is formally identical to the one of Tam and Auriault (T&A)[1] assuming that the velocity fluctuations of the acoustic sources is negligible if compared with the mean flow velocity. The RPM method has also some adjustments in the relations to gather the necessary parameters from the turbulence statistics of the RANS. This adjustments are necessary because the original (T&A) derived spectra yields Strouhal similarity whereas the RPM method yields Helmholtz similarity. To be equivalent the RPM method is adjusted to be Strouhal similar. For the derivation of the spectra refer to Ewert and Neidfeld[5] and (T&A).[1] The source term q_p is set to be equivalent to the (T&A) source term

$$q_p \equiv \frac{Dq_s}{Dt}, \tag{2}$$

the equivalent cross correlation equation for the RPM method model is

$$\langle q_p(x,t)q_p(x+r,t+\tau)\rangle = \hat{R} \times \exp\left\{ -\frac{|\tau|}{\tau_s} - \frac{\ln 2}{l_s^2}[(\xi - u_j\tau)^2 + \eta^2 + \zeta^2]\right\} \tag{3}$$

where

$$\hat{R} = \frac{\hat{q}_s^2}{c^2\tau_s^2}. \tag{4}$$

(T&A) define two types of noise generation sources in turbulent jets. Noise from large turbulent structures (F-Spectrum) and noise from fine-scale turbulence (G-Spectrum) which have different generation mechanisms and different areas of influence. The (T&A) model is for the fine-scale turbulence noise. τ_s is the characteristic decay time of the fine-scale turbulence and l_s the characteristic size. The variance of the source $\hat{R}$ is specified by $\hat{q}_s^2$ which is the kinetic energy of the fine-scale turbulence per unit volume and c is a constant. The variables ξ, η and ζ are the relative distance between two points and u_j represents the jet convective velocity. From the RANS simulation solution using a two-equation model or Reynolds Stress Model l_s is calculated

$$l_s = c_l\frac{k^{\frac{3}{2}}}{\epsilon} \tag{5}$$

where $c_l = 0.273$, k and ϵ are the turbulent kinetic energy and the turbulent dissipation rate from the RANS respectively. τ_s is calculated as

$$\tau_s = c_\tau\frac{k}{\epsilon}, \tag{6}$$

DOI: 10.13009/EUCASS2019-613

with $c_\tau = 0.233$. The fluctuating component q_p which is the source term in the LEE equations is generated by convolving a spatiotemporal convective white-noise $\mathcal{U}$ with a filter kernel,

$$q_p = \int_{V_S^n} \hat{A} G(\boldsymbol{x} - \boldsymbol{x'}) \mathcal{U}(\boldsymbol{x'}, t) d^n x'. \tag{7}$$

G is a Gaussian filter kernel and n indicates the dimension of the Problem. V_S^n is the considered source region. $\hat{A}$ models the variance of q_p with

$$\hat{A} = \left(\frac{4 \ln 2}{\pi}\right)^{\frac{n}{4}} \sqrt{\frac{\rho_0 \hat{R}}{l_s^n}}. \tag{8}$$

From a practical point of view the area where sources are located is the so called patch. The area is typically modeled with a similar width of the nozzle exit $y/D = 1$ and a length up to $x/D = 30$. D is the jet exit diameter. An example of the the patch location and dimension is shown in Figure 2. The patch contains all the necessary variables derived from the RANS simulation to calculate the q_p. The trayectories along which the source particles are moving with the underlying axial flow velocity is also defined in the patch.

2.2 CAA Solver

The numerical results are obtained using the acoustic sources described in the previous section as input for the DLR CAA Solver PIANO. The governing equations are solved on the basis of a finite difference method using a structured, curvilinear coordinate system. In PIANO for azymuthal problems the LEE are implemented as complex Fourier series. The user chooses the number of terms or modes the series should have and PIANO solves each mode of the series separately. Later the contribution of each term is added to the final solution. It is important to have enough modes in order to have suffient frequency resolution of the results. This method allows to increase the efficiency of parallelization of the problem.

3. Numerical Set-Up

The RANS simulation was performed using the DLR solver Tau using the Wilcox Reynolds Stress model[12] with turbulence shock correction. An alternative k-ω turbulence model was not taken into account, due to the overprediction tendency of flow separation in the nozzle. The turbulence shock correction is necessary for any turbulence modeling due to the overprediction of turbulent energy inherent to RANS turbulence models, for more details about the turbulence model for shock-turbulence interaction refer to Karl et al.[6] This turbulence model proved to perform best in both RANS and acoustic simulation. Refer to Costa et al.[3] The axis symmetry property is used in both the RANS and the CAA simulations to reduce the numerical effort. The RANS of the TOP test case simulation has a mesh with $1.02 \cdot 10^6$ points. The RANS mesh for the TIC test case has $1.22 \cdot 10^6$ points. The simulation domain area for both test cases is about 33 exit diameters in axial direction and 15 exit diameters in radial direction. The RPM patch area for the for the TIC test case is identical to the TOP test case. The position of the microphones is shown in Figure 2. The pressure profile realized in the experiments is shown in Figure 3. In both experiments the profile has a plateau of a few seconds at maximal pressure. The operating point at this plateau was used as boundary condition for the RANS simulation. The nozzle to pressure ratio ($NPR = p_0/p_a$) applied for the simulation is 58.24 for TOP test case and 60.1 for the TIC. For the CAA computations a structured mesh with $4.5 \cdot 10^5$ points was used. The boundary conditions for the CAA computation is acoustic wave absorbing for the ambient boundaries and acoustic reflecting euler wall for the axis symmetric walls. For the nozzle walls acoustic reflecting no slip walls was applied.

4. Experimental Set-Up

The experimental data was acquired in tests conducted at DLR Lampoldshausen in the cold flow test facility P6.2. For each experiment 11 microphones at different positions were simultaneously measured. The data acquisition system was a Brüel & Kjaer. An overview of the microphone names their position and their angle respect the center of the nozzle exit plane is shown in Figure 2. For all the microphone signals an antialiasing filter was applied. The TOP experiments were measured at sampling rate of 8192 Hz whereas the TIC experiments were measured with 16384 Hz. Parallel to the microphone measurements a schlieren video was recorded during the complete experiments. Both nozzles used as test case data have similar geometry and operation parameters. One important geometry difference is the diameter of the throat, the TOP nozzle has a throat diameter of 22 mm and the TIC has 20 mm. An overview showing a comparison

DOI: 10.13009/EUCASS2019-613

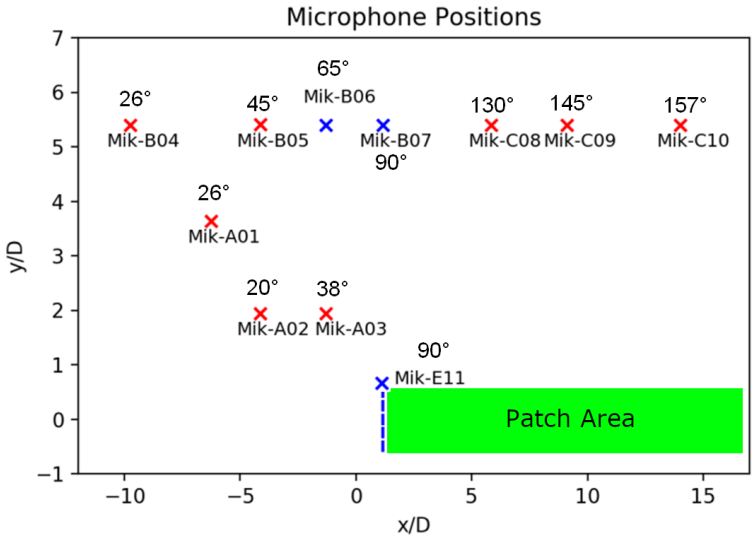

Figure 2: Microphone position in the simulation and the experiment relative to the nozzle exit diameter with the angle respect nozzle exit plane (blue line). Microphones between in the area between 50° and 110° in blue, RPM-Patch area in green

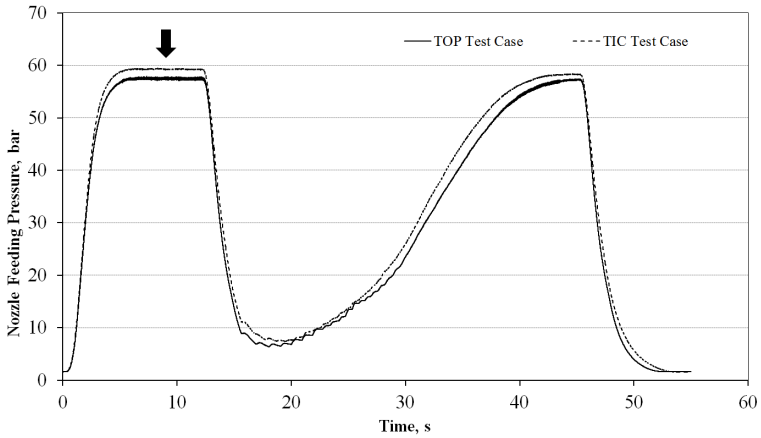

Figure 3: Nozzle pressure test profile for the TOP (continuous line) and TIC (discontinuous line) test case. The arrow indicates the operating point used for the simulations

of both experimental test cases is shown in Table 1. Important for the evaluation is the Strouhal number. In this work the Strouhal number is formed

$$S_{tr} = \frac{fD_e}{u_j}, \tag{9}$$

where f is the frequency, D_e is the nozzle exit diameter and u_j the jet velocity shown in Table 1. For more detailed information about the experimental set-up refer to Stark et al.[9]

5. RANS Results

The RANS result are important as first step in order to gather the turbulence statistics for the CAA computation. It is important to choose the appropriate turbulence model and also to check that the form, and the characteristics of the simulated jet are as similar as possible to the experiment. In order to check the characteristics of the jet, a comparison between the schlieren images and the Mach number distribution in the simulation was performed. The comparison is shown in Figure 4. The simulation and the experiments show a very good agreement for the positions of the shocks and their geometry.

DOI: 10.13009/EUCASS2019-613

Table 1: Comparison of the experimental data between the TOP and the TIC test case. Refer to Stark et al.[9]

		TIC	**TOP**	**Ratio**
Design Mach number	M_D	5.15	6.78	0.756
Exit wall Mach number	M_e	4.38	4.43	0.999
Oblique shock angle, °	s	26.1	24.2	1.0785
Jet Mach number	M_j	3.11	3.29	0.945
Pressure reduction, %	p_{02}/p_{01}	75.8	80.8	0.938
Jet pressure ratio	p_j/p_a	1.054	0.854	1.2342
Jet velocity,m/s	u_j	606.9	640.6	0.947
Nozzle exit diameter,m	D_e	$9.05 \cdot 10^{-2}$	$9.80 \cdot 10^{-2}$	0.9235
Ratio diameter/velocity,s	D_e/u_j	$1.491 \cdot 10^{-4}$	$1.529 \cdot 10^{-4}$	0.975
Frequency prediction,Hz	f_{Tam}	681	622	1.0948

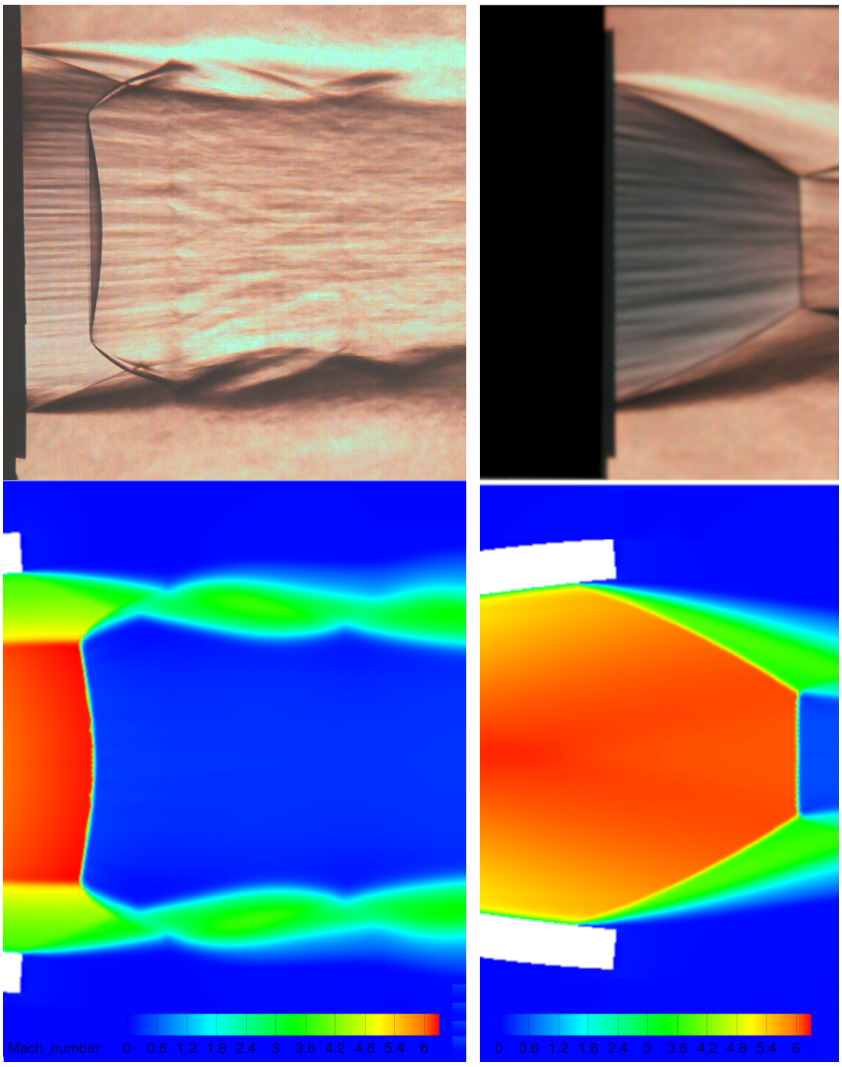

Figure 4: Comparison between Mach number distribution (bottom) and schlieren (top) for the TOP (left) and the TIC (right)

6. CAA Results

During post-processing the acoustic simulation results were handled as similar as possible to the experimental data collection and processing. The data of the simulations was resampled to 8192 Hz for the TOP test case and to 16384 Hz for the TIC test case. The postprocessing was achieved with python scripting. A list of the CAA-Simulations with

DOI: 10.13009/EUCASS2019-613

computational data is presented in Table 2. For the TOP simulation 0.918 ms of simulation were calculated per hour using 47 CPUs. For the TIC simulation 0.462. The reason for this difference is that the simulations had different time step sizes. The time step of the TIC was approximately half of the size the time step of the TOP. The total duration correlates linearly with the time step size therefore it is always advisable to choose the biggest time step possible that the numerical stability allows.

Table 2: Overview of the performance data of the simulations

Simulation	**Sim. Time, ms**	**CPUs**	**Duration, hours**	**Calculation speed,** $\frac{ms}{hours}$
TOP	224.8	47	244.76	0.918
TIC	252	47	545.18	0.462

6.1 Spectral Analysis

A Fast Fourier Transform (FFT) was applied to all microphone data and compared to simulation data. The FFT was performed by taking 10 intervals with a length of 20 ms with 50% overlapping and averaging them after performing the FFT. The microphone E11 will not be taken into account for the evaluation since some fixation problems were detected during the experiment making the data unreliable. The FFT analysis is shown in Figure 6 and 7 for the TOP and the TIC test case respectively. The frequency was resolved up to $S_{tr} = 0.62$ for the TOP and up to $S_{tr} = 1.2$ for the TIC test case. The TOP test case shows a very good agreement for the microphones A03, B05, B06, C08. The microphones, which are in the area where the T&A theory produces best results, are B06, B07 and E11 (see Figure 2). The simulations tend to produce good data at the sides of the jet plume and worse results very downstream and high upstream from the jet. The same tendency is observable for the TIC test case as well. For the TIC test case the best match between simulation and experiment is given for the microphones A03, B06, B07 and C08. For the TIC test case it is clearly visible that there is a peak frequency at $S_{tr} = 0.2$. The peak is clear in the microphones A02-C08. This was a screech tone which was detected during the experiments. For the TOP test case there were also some dominant frequencies ($S_{tr} = 0.25$ and $S_{tr} = 0.32$) in the experiment, they were however not so strong as in the TIC test case. In both cases for the microphones C09 and C10 it is clear that the experiments spectrum is higher than the simulated spectrum. Tam et al.[2] describe two different noise types for jet mixing noise with different generation mechanisms. The first one is coherent and dominant in the downstream sector of the jet, and it is generated by large scale turbulent structures. The second one is more random with a large frequency bandwidth and it is dominant on the sidelines of the jet. The second noise source is generated by small scale turbulent structures. In Figure 8 and 9 the Power Spectrum Density (PSD) waterfall diagram for the TIC and TOP respectively is shown for all microphones except E11. The microphones C09 and C10 show clearly a different PSD compared to the rest of the microphones. C09 and C10 have coherent structures in frequency whereas the other microphones have a more flat distributed frequency. The position of the microphones and the evaluated results seem consistent with the two types of noise sources described by Tam et al.[2] This coherent structures could be what Tam[10] identifies as Mach wave radiation, which are large turbulent structures formed at the shear layer of a supersonic jet. The results of simulation and experiment show that the CAA computation is not able to reproduce dominant frequencies such as screech tones observed in the experiments. The poorest numerical results were found in the downstream area of the jet for the microphones C09 and C10. The results of the microphones very upstream of the nozzle exit area, microphones A01 and B04, are also not very satisfactory. A good match between the spectra of the simulation and experiment can be observed in the sidelines of the jet.

6.2 Overall Sound Pressure Level

The Overall Pressure Level (OASPL) was analyzed for both TOP and TIC test cases. The OASPL is represented in polar coordinates and it is shown in Figure 5. For both test cases the OASPL in the tests is clearly higher than the simulation for high angles (downstream from the nozzle exit). For very low angles (uptstream) the OASPL of the experiment tends to be higher than in the simulation. The best match is observed between 45° and 135°. The agreement between experiment and simulation is for the TOP nozzle better than for the TIC nozzle. A possible explanation for the different agreement in the results of the TIC and the TOP test cases could be the strong screech tone observed in the TIC test case. The screech tone increases the total emitted acoustic loads generating a higher OASPL for all microphones as observed in the TIC test case. Since the used numerical method can not reproduce screech tones, it is expected that the OASPL of the TIC simulation is lower than in the experiment.

DOI: 10.13009/EUCASS2019-613

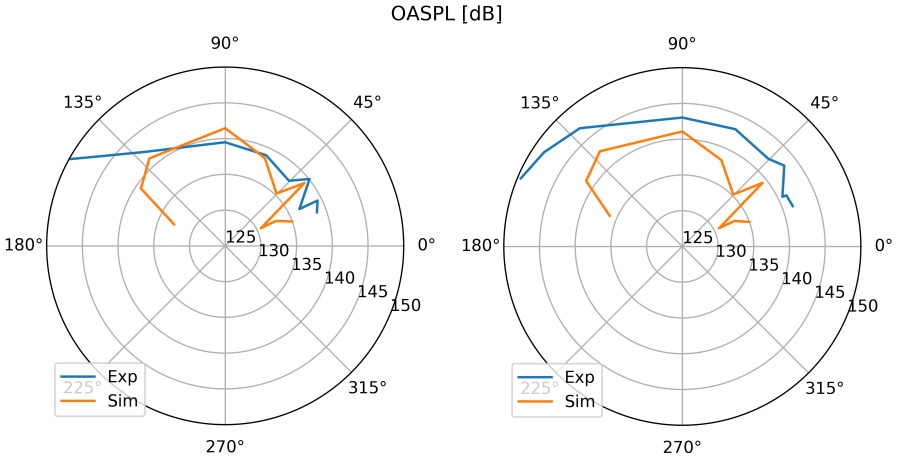

Figure 5: OASPL polar diagramm for the TOP (left) and the TIC (right) test cases

7. Conclusion and Outlook

Two test cases were simulated acoustically using PIANO and the RPM-Method.[4] The test cases have jet Mach numbers of 3.29 and 3.11 for the TOP and the TIC respectively. The model of T&A[1] is only tested for jet Mach numbers up to 2. The results show that quality of the agreement between simulation and experiment depends on the spatial distribution of the microphones. The numerical results for the microphone positions very downstream and upstream from the nozzle exit show unsatisfactory results. The screech tones and other dominant frequencies observed in the experiment can not be reproduced with the used numerical method. The analyzed spectra distributions show the greatest disagreement for microphones very downstream from the nozzle exit. This is coherent with the underlying theory, which is a theory for the noise generation by fine-scale turbulence. Large scale turbulence structures are the dominant noise source downstream from the nozzle exit. Good numerical results were achieved at the sidelines of the jet, where the fine-scale turbulence is the dominant noise generation mechanism according to T&A. Due to the economic numerical resources needed to achieve the numerical results it is thinkable to apply this numerical method for rocket engine test benches where the plume is usually covered by a guide tube damping the effects of the noise produced downstream from the nozzle exit. A similar scenario may be given at the launch pad as well. Assuming that the plume is covered by a guide tube, where water is injected, so that the noise generated downstream is damped, then the noise generated in the sidelines of the plume may become the dominant noise source, making the method suitable to perform acoustic calculations.

8. Acknowledgments

The present work was conducted in the framework of the German Aerospace Center (DLR) project TAUROS (TAU for Rocket Thrust Chamber Simulation) focusing on the qualification and advancement of the DLR flow solver TAU for liquid rocket thrust chamber applications. The financial support mof the DLR Space Research Programmatic is highly appreciated. I also want to thank Jürgen Dierke and Andrej Neidfeld from DLR Technical Acoustics Department for his technical support using PIANO.

References

[1] Tam C. and Auriault L. Jet mixing noise from fine-scale turbulence. *AIAA Journal, vol. 37, pp. 145-153*, 1999.

[2] Tam C., K. Viswanathan, K. Ahuja, and J. Panda. The sources of jet noise: experimental evidence. *J. Fluid Mech. (2008), vol. 615, pp. 253-292*, 2008.

[3] E. Costa Ruiz, R. Stark, C. Genin, and M. Oschwald. Acoustic emission prediction of supersonic cold flow jets using a cfd-caa hybrid method. In *Space Propulsion 2018*, 2018.

[4] R. Ewert. Rpm - the fast random particlemesh method to realize unsteady turbulent sound sources and velocity fields for caa applications. *13th AIAA/CEAS Aeroacoustics Conference, AIAA 2007-3506*, 2007.

DOI: 10.13009/EUCASS2019-613

[5] R. Ewert and A. Neifeld. A 3-d modal stochastic jet noise source model,. *17th AIAA/CEAS Conference, Portland USA*, 2011.

[6] S. Karl, J.-P. Hickey, and F. Lacombe. Reynolds stress models for shock -turbulence interaction. *Proceedings of the 31st International Symposium on Shock Waves, Nagoya, JP*, 2017.

[7] S. Langer, A. Schwoeppe, and N. Kroll. The dlr flow solver tau - status and recent algorithmic developments. *AIAA Paper 2014-0080*, 2014.

[8] A. Neifeld and R. Ewert. Jet mixing noise from single stream jets using stochastic source modeling. *17th AIAA/CEAS Conference, AIAA 2011-2700*, 2011.

[9] R. Stark, D. Schneider, J. Martin, and S. General. Experimental study on jet acoustics of subscale rocket nozzles with a different divergent contour design. *EUCASS, 8th European Conference for Aerospace Sciences, No. 514, 1-4 July, Madrid, Spain*, 2019.

[10] C. Tam. Mach wave radiation from high-speed jets. *AIAA Journal, Vol. 47, No. 10*, 2009.

[11] S. Tsutsumi and K. Terashima. Validation and verification of a numerical prediction method for lift-off acoustics of launch vehicles. *Trans. JSASS Aerospace Tech. Japan, Vol. 15, pp. 7-12*, 2017.

[12] D.C. Wilcox. *Turbulence Modeling for CFD*. DCW Industries Inc. La Canada CA, 2006.

DOI: 10.13009/EUCASS2019-613

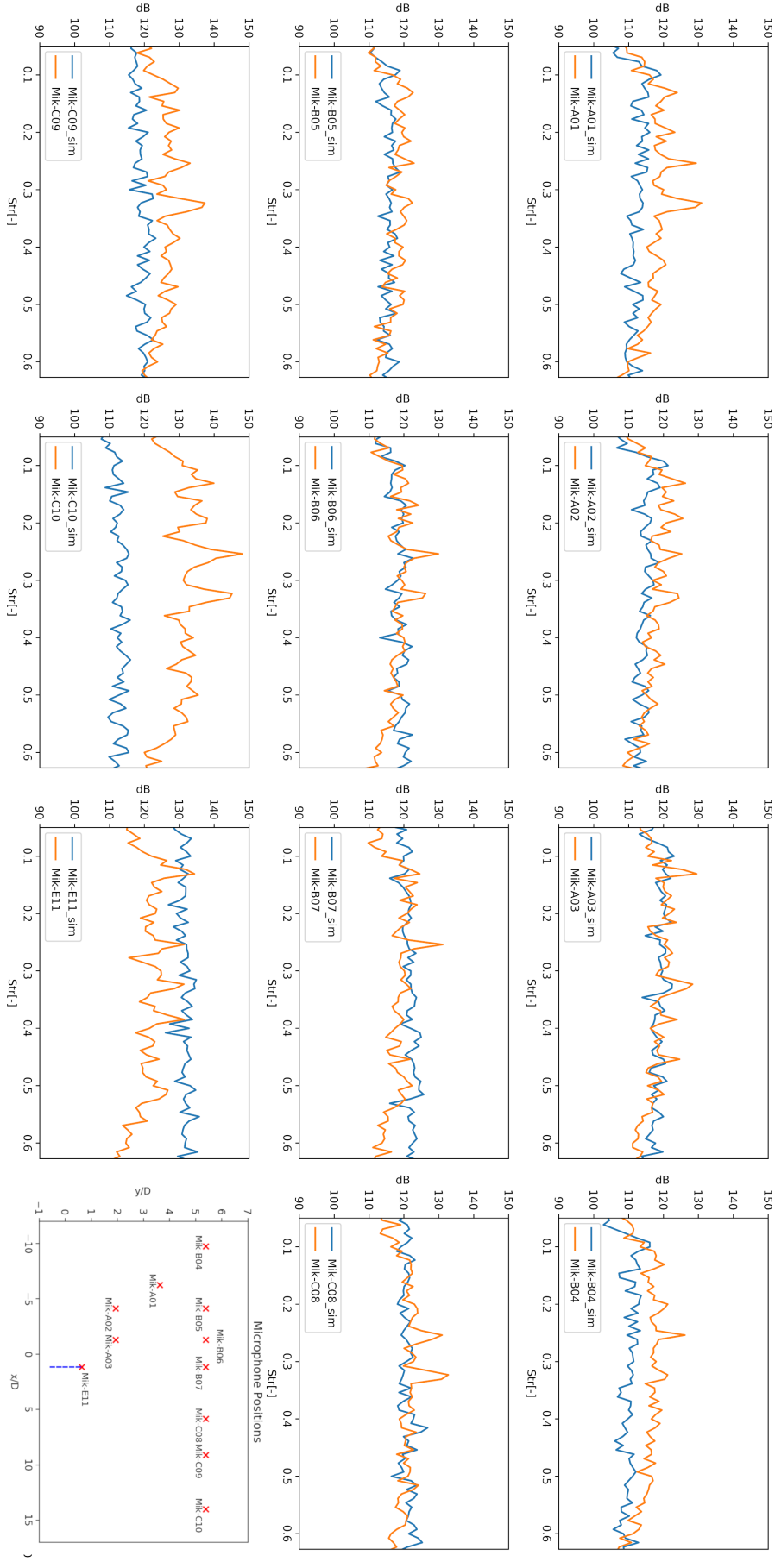

Figure 6: TOP nozzle FFT

DOI: 10.13009/EUCASS2019-613

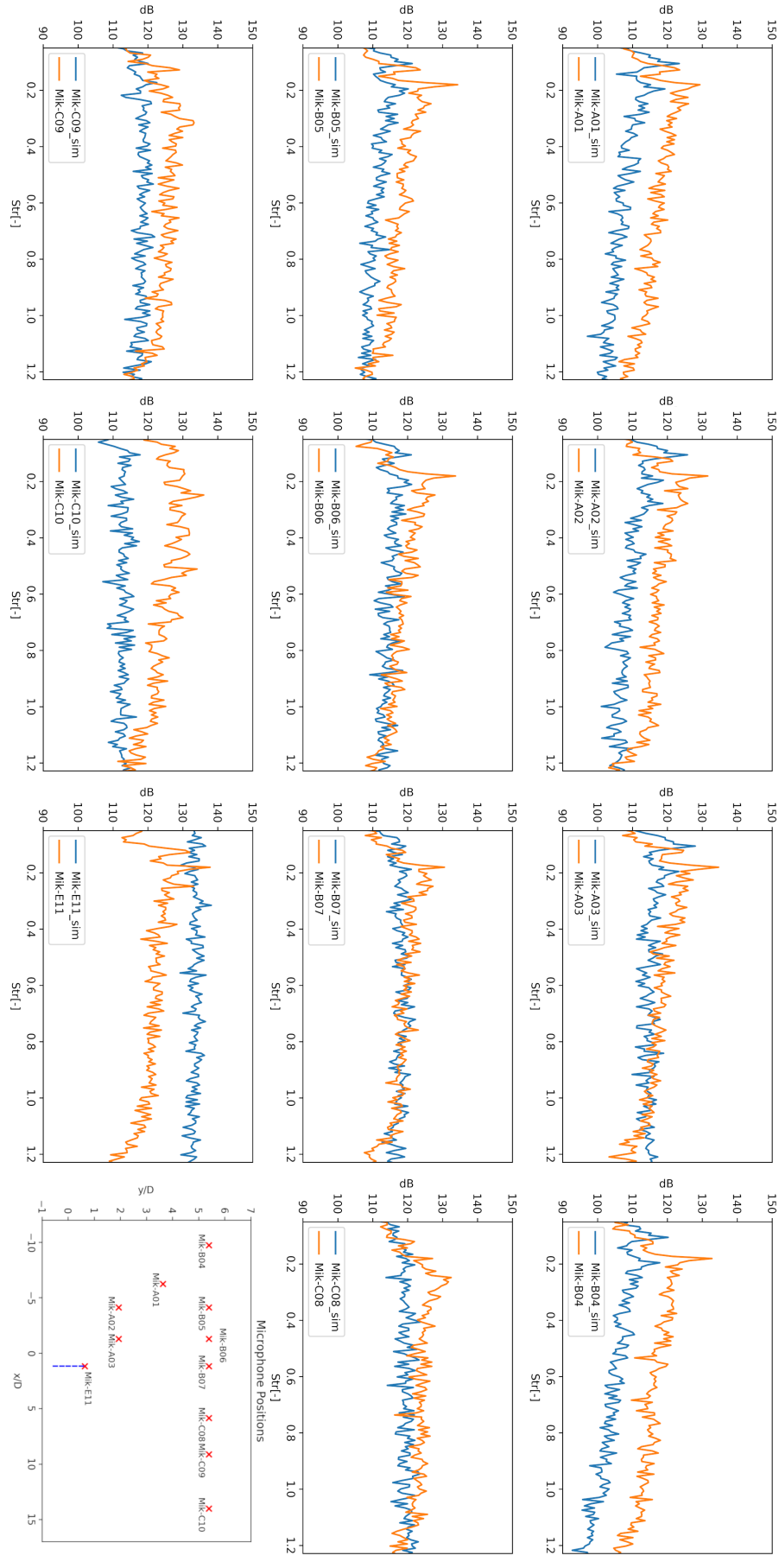

Figure 7: TIC nozzle FFT

DOI: 10.13009/EUCASS2019-613

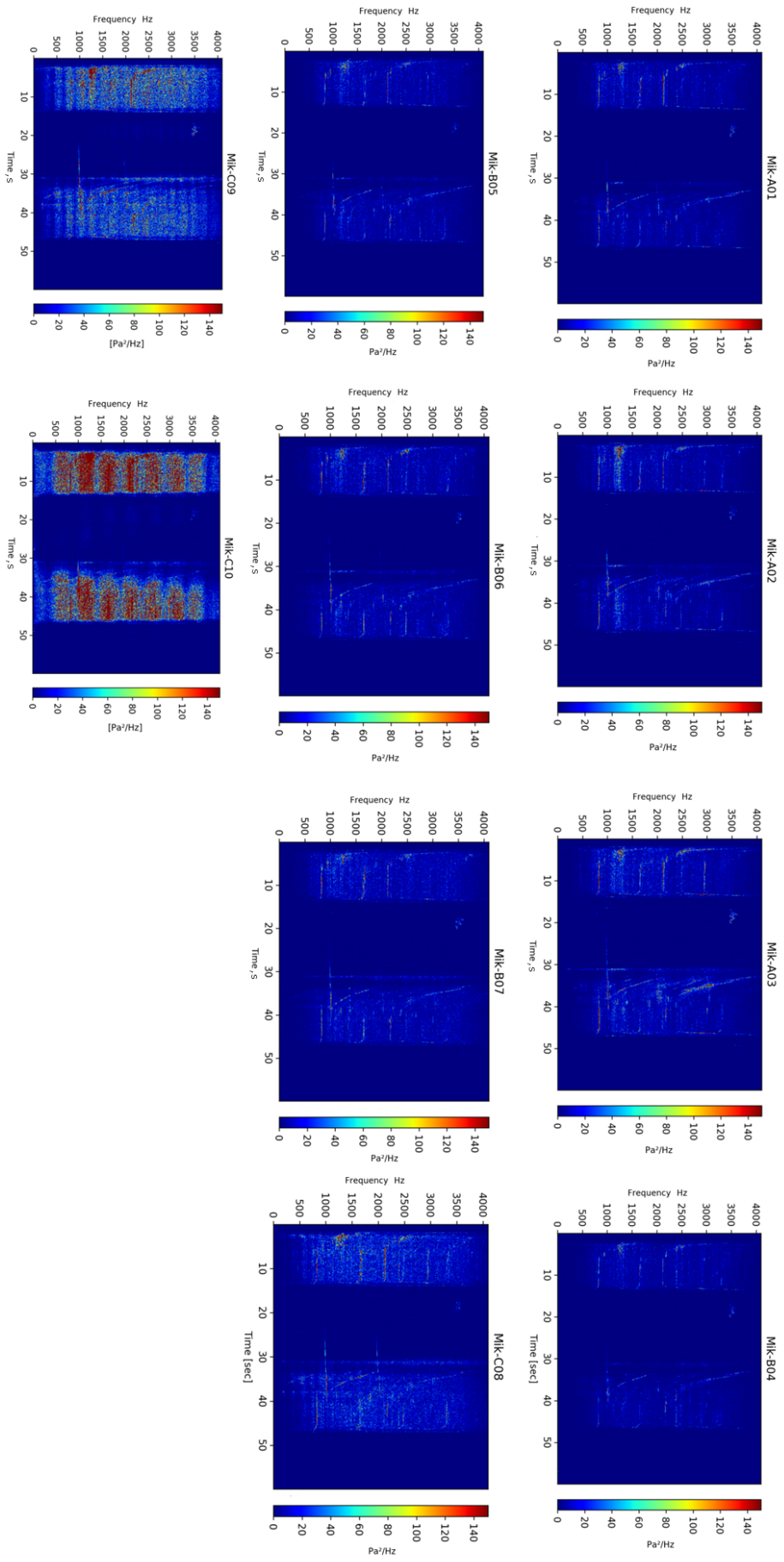

Figure 8: TOP nozzle PSD waterfall diagramm

DOI: 10.13009/EUCASS2019-613

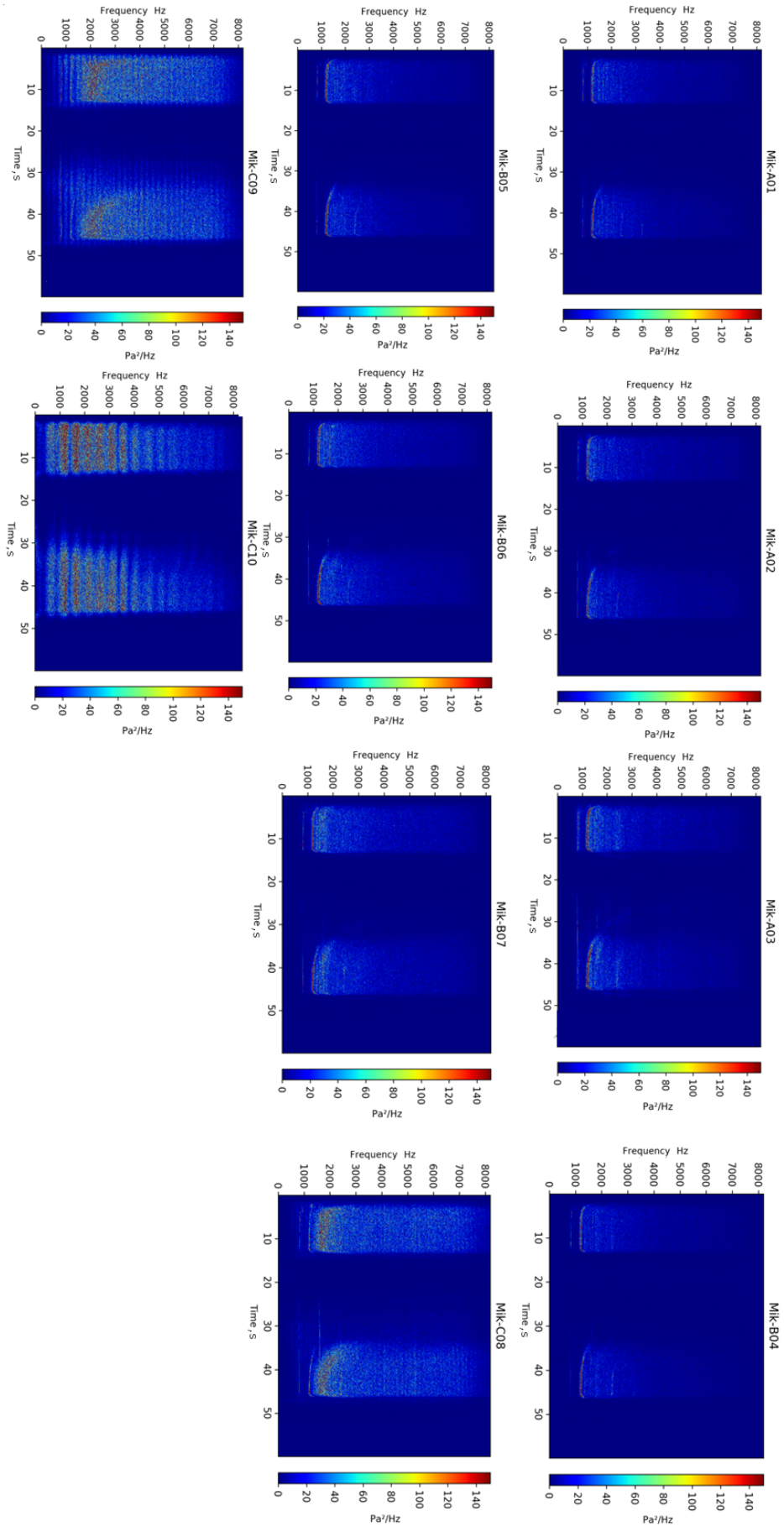

Figure 9: TIC nozzle PSD waterfall diagramm